



# Cycling and atmospheric exchanges of selenium in Canadian subarctic thermokarst ponds

Laurent Lancelleur · Emmanuel Tessier · Maïté Bueno · Reinhard Pienitz · Frédéric Bouchard · Christophe Cloquet · David Amouroux

Received: 8 January 2019 / Accepted: 10 September 2019 / Published online: 21 September 2019  
© Springer Nature Switzerland AG 2019

**Abstract** The levels and speciation of dissolved, particulate and gaseous Se have been measured in five thermokarst ponds in a sporadic and discontinuous permafrost region of northern Québec (Canada) during summer oxygen stratification. Evolution of Se concentrations with depth was investigated in sediment cores collected in three different ponds. The potential for inorganic Se transformation in natural pond waters was investigated by experimental incubations of isotopic species-specific tracers of selenite and selenate. Experimental and monitoring observation revealed that high dissolved carbon concentration, suspended particle matter concentration, heterotrophic activity and periphytic biofilms have a significant role in the formation of gaseous selenium species. In

sediment, Se is mainly associated with organic matter in the concentration range 0.14–1.6 mg kg<sup>-1</sup>. Despite low outgassing rates of volatile Se toward the atmosphere (1–97 ng Se m<sup>-2</sup> day<sup>-1</sup>), the large surface occupied by ponds in northern Canada may lead to important exchange rates (ca. 1 ton year<sup>-1</sup>) at the global scale. Detailed measurements of Se speciation, including volatile compounds, and its reactivity toward heterotrophic activity in selected thaw ponds from the Canadian Subarctic provides new insight to better constrain the biogeochemical pathways leading to Se removal from the water column via atmospheric gas exchange and sediment accumulation.

**Keywords** Flux · Permafrost · Selenium · Subarctic · Thermokarst · Volatile

---

Responsible Editor: R. Kelman Wieder.

---

L. Lancelleur · E. Tessier · M. Bueno · D. Amouroux  
CNRS / Univ Pau & Pays Adour / E2S UPPA, Institut des sciences analytiques et de physico-chimie pour l'environnement et les matériaux – MIRA, UMR5254, 64000 Pau, France  
e-mail: laurent.lancelleur@univ-pau.fr

R. Pienitz · F. Bouchard  
Département de Géographie et Centre d'études nordiques, Université Laval, Québec City, QC G1V 0A6, Canada

C. Cloquet  
CRPG-CNRS, 15 rue Notre Dame des Pauvres, 54501 Vandœuvre les Nancy, France

## Introduction

Permafrost represents 24% of the continental surface in the northern hemisphere and more than 50% of Canadian landscapes (Brown et al. 1998; Zhang et al. 2008). Over the last 50 years, climate warming has already induced decreases of permafrost area in subarctic Alaska (Riordan et al. 2006) and in the eastern Hudson Bay region in the order of 25% in the northern part (Vallée and Payette 2007) and up to 80% in the southeastern part (Payette et al. 2004). According to the latter study, Canadian permafrost will

disappear completely in the coming decades should the loss rates remain as high as those of the 1990s. As a consequence of rapid permafrost thaw, numerous thermokarst ponds and lakes formed in topographic depressions (Pienitz et al. 2008), a process that is underestimated and may amplify in future years (e.g. Bouchard et al. 2014). These freshwater ecosystems concentrate atmospheric deposition, ground leaching and ice thaw waters as well as associated contaminants (Pienitz et al. 2008). Recent focus on selenium (Se) behavior in natural wetlands has pointed to the possibility of volatile Se species being released over large areas (6–11% of the world's land area) and, consequently, their contribution to widespread Se distribution in the environment and biota (Vriens et al. 2014; Zhang and Moore, 1997).

In the context of global warming, very little is known about the contribution of thawing and erosion of ice-rich permafrost landscapes throughout northern regions to Se enrichment. The spatial and temporal variation of Se in permafrost areas of western Siberian lowlands has been studied recently (Pokrovsky et al. 2018), but Se cycling in permafrost of Canadian territories has rarely been investigated.

Subarctic environments are remote areas located at far distances from many natural and anthropogenic contaminant sources. However, the atmosphere is known to represent an important transient reservoir in the Se cycle (Amouroux et al. 2001; Cutter and Church 1986; Lag and Steinnes 1974; Ross 1985; Wen and Carignan 2007, 2009). Atmospheric transport and deposition of Se from natural sources (crustal weathering, volcanoes, sea salt, and the continental and marine biospheres; Blazina et al. 2017; Mosher and Duce 1987; Nriagu 1989; Nriagu and Pacyna 1988; Ross 1985) as well as emissions from anthropogenic activities (mainly mining, smelting and refining of chalcophilic ores and fossil fuel combustion; Ross 1985; Lemly 1994, 2004) are primary mechanisms by which Se may be distributed throughout the environment, impacting remote areas including the Arctic (Beavington et al. 2004; Bennett 1995; Cutter and Church 1986; Cutter and Cutter 2004; Kagawa et al. 2003; Maenhaut et al. 1989; Nriagu and Dawidson 1986; Wen and Carignan 2007).

Wen and Carignan (2009) observed that atmospheric Se emitted by marine phytoplankton is often associated with sub-micron sea salt particles containing chlorine (Cl) before deposition on coasts.

Associated with increasing anthropogenic inputs in the atmosphere and following deposition to the ocean, Se concentration has increased in the upper ocean waters over the past 30 years (Mason et al. 2018). The authors used the Se/Cl ratio variation in epiphytic lichens to estimate the influence of marine biogenic Se, and concluded that the high ratio measured in the Hudson Bay region may be due to i) a higher production rate of volatile Se compounds by plankton in this area, and/or ii) the contribution of other natural or anthropogenic atmospheric Se sources (Wen and Carignan 2009).

In the mid-1990s, emissions of selenium from major anthropogenic sources in North America were second in world ranking with 1000 tons year<sup>-1</sup> (Pacyna and Pacyna, 2001). Even if atmospheric emissions of Se are expected to remain more or less stable over the next 25 years based on international treaties on global environment and gas emissions (Cofala et al. 2007), Arctic and Subarctic regions will experience rising mining exploration/exploitation and oil/gas industrial activities over the coming decades (ACIA 2004). At a global scale, if mining site pollution is obvious, diffuse pollution from atmospheric transport is not fully apparent and understood. Only a small proportion (approx. 49% Cu, 15% Pb, 23% Zn and 9% Cd) of total emissions from a smelter reaches the ground within a 50 km radius around chimney stacks (Telmer et al. 2004). Isotope tracing confirmed Pb emissions more than 500 km away from the original refinery (Carignan and Gariépy 1995) and up to 10<sup>6</sup> km<sup>2</sup> according to numerical models (Telmer et al. 2004).

The simultaneous impacts of climate change and increasing land exploitation in the Arctic on biogeochemical uptake, transformation, food chain accumulation and potential atmospheric release of Se remain poorly known aspects that limit both efficient hazard assessment and pollution control. Moreover, understanding biogeochemical processes occurring in this particular environment is essential to predict the distribution of selenium at a global scale (Winkel et al. 2012).

The objectives of the present study are the evaluation of current Se content, chemical speciation and specific biogeochemical pathways in subarctic thaw ponds, an ecogeosystem submitted to rapid change and exhibiting challenging Se trace concentrations (below 0.1 µg L<sup>-1</sup>). The main outcomes of this work are the

direct measurement of Se speciation and reactivity in selected thaw ponds from the Canadian Subarctic and the potential processes leading to its atmospheric volatilization or sediment accumulation.

## Materials and methods

### Sampling

Thermokarst ponds located inland from the southeastern coast of Hudson Bay, near the hamlet of Kuujuarapik-Whapmagoostui in subarctic Québec, Canada (Fig. 1), were chosen as the study sites among ponds and lakes monitored by the CNS (Centre for Northern Studies) network. Ponds were relatively inaccessible and largely undisturbed by anthropogenic activities throughout most of their history. The sites were located along a south-north transect along the eastern Hudson Bay coast and representative of sporadic permafrost to discontinuous permafrost for the northern site (Allard and Seguin 1987; Payette and Rochefort 2001). Ponds are developed over marine silty clay and littoral sand deposits in topographic depressions (Hillaire-Marcel 1976; Saulnier-Talbot and Pienitz 2001) and overlying glacially eroded granitic/gneissic bedrock of Precambrian age. Sites

were coded according to the valley name where ponds were located, namely the Sasapimakwananiskiw River valley (SAS1A), the Kwakwanikapistikw River valley (KWAK1, 2, 6, 12, 16), the Sheldrake River valley (BGR-A) and the Nastapoka River valley (NAS1A).

Sedimentological and geomorphological processes have been investigated in detail over the last 50 years, particularly at the KWAK site presenting the most representative thermokarst ponds (Bouchard et al. 2011, 2014). The KWAK ponds (1, 2, 6, 12, 16), BGR-A and NAS1A originated from the thawing of lithalsa (i.e. mineral mounds) while the SAS2A pond derived from the thawing of palsas (i.e. organic mounds). The vegetation cover of the latter was dominated by grasses (*Carex*) and mosses (*Sphagnum*) instead of shrubs and sparse trees at other sites (Calmels et al. 2008). The SAS2A, KWAK (1, 2, 6, 12, 16) and BGR-A ponds were situated in sporadic and highly degraded permafrost landscapes. The NAS1A pond had the particularity to be located at the limit between sporadic permafrost and the less degraded, discontinuous permafrost zone.

Sampling occurred during the frost-free period (mid-May to end of September). Each pond was stratified, exhibiting steep gradients with an oxic epilimnion from surface to mid-depth (1 m to 2 m

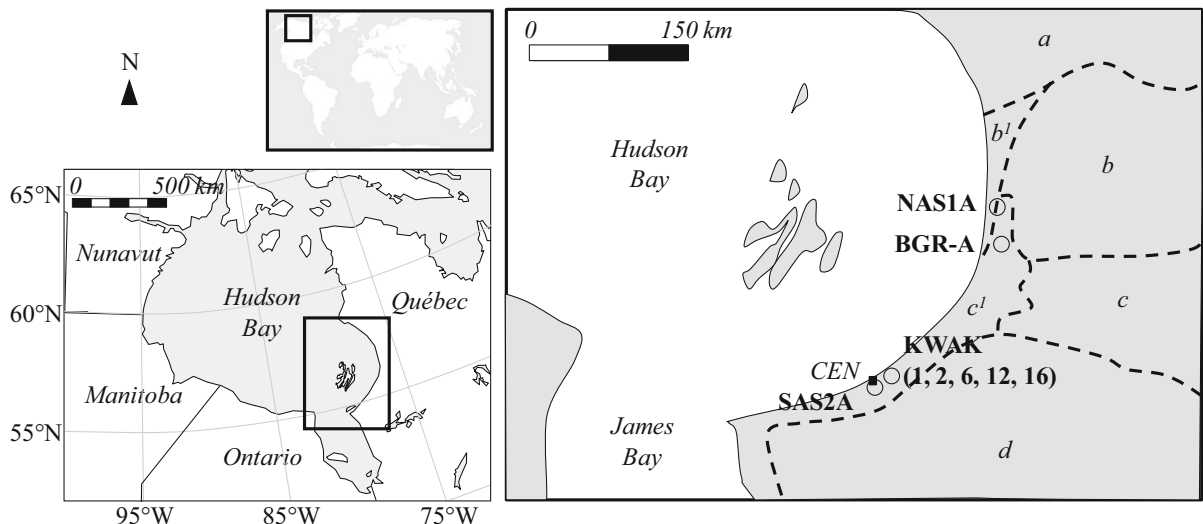


**Fig. 1** Thermokarst ponds location (round) of sampled in the southeastern Hudson Bay coastal area. CEN Centre for Northern Studies. (a): Continuous permafrost (> 90% of land surface). (b): Discontinuous permafrost (50–90% of land surface). Sub-zone b: Plateaus and mounds in clayey silts of Tyrrell Sea. (c):

Sporadic permafrost (10–50% of land surface). Sub-zone c: Palsas overlying fine Tyrrell Sea sediments. (d): Isolated permafrost (< 10% of land surface). Modified from Bhiry et al. (2011) and Coulombe et al. (2016)

depth) and an oxygen depleted-hypolimnion (Table 1). The stratification was less marked in the BGR-A pond, which was located close to the Sheldrake River. Sampled thermokarst ponds displayed significantly different water colors from white to black and also substantial differences in SPM (suspended particulate matter) concentrations. In this

particular environment, water color is used as an indication of pond age (Bouchard et al. 2011; Laurion et al. 2010; Watanabe et al. 2011). Indeed, with age, terrestrial and aquatic vegetation growth releases dissolved organic carbon in pond waters and stabilizes shores. On the contrary, decreasing input in mineral matter allows the settling of fine particles and

**Table 1** Measurements from the five sampled thermokarst ponds

	SAS2A	KWAK1	KWAK12	BGR-A	NAS1A
Lat	55°13' N	55°20' N	55°20' N	56°36' N	56°55' N
Long	77°42' W	77°30' W	77°30' W	76°12' W	76°22' W
Water column					
Depth (m)	2.20	1.60	2.50	3.00	2.50
Secchi depth (m)	0.75	1.5	1.5	1.15	0.05
Temp (°C)					
Surf.	14.4	15.5	14.7	<i>nd</i>	<i>nd</i>
Depth	5.6	8.7	8.3	<i>nd</i>	<i>nd</i>
O <sub>2</sub> (mg L <sup>-1</sup> /%)					
Surf.	6.4/64	9.7/98	8.5/85	9.7/91	10/89
Depth	0.3 (2)	0.6 (6)	0.3 (3)	7.8 (74)	2.4 (20)
SPM (mg L <sup>-1</sup> )					
Surf.	3	38	<i>nd</i>	3	470
Depth	7	42	15	5	600
Se <sub>TOTAL</sub> (ng L <sup>-1</sup> )					
Surf.	56 ± 3	107 ± 15	<i>nd</i>	35 ± 1	85 ± 9
Depth	67 ± 13	98 ± 5	56 ± 1	24 ± 9	101 ± 5
Se <sub>&lt;0.22</sub> (ng L <sup>-1</sup> )					
Surf.	46 ± 15	63 ± 12	<i>nd</i>	35 ± 8	61 ± 12
Depth	50 ± 12	56 ± 12	45 ± 6	18 ± 7	67 ± 18
Se <sub>G</sub> (DMSe, pg L <sup>-1</sup> )					
Surf.	3.2	1.5	<i>nd</i>	4.1	31
Depth	2.9	2.0	2.1	2.9	55
Se <sub>SPM</sub> (mg kg <sup>-1</sup> )					
Surf.	3.3	1.2	<i>nd</i>	<i>bdl</i>	0.05
Depth	2.4	1.0	0.73	1.2	0.06
Sediment					
POC (% mg mg <sup>-1</sup> )	32 ± 0.1	3.4 ± 0.0	4.1 ± 0.0	1.1 ± 0.0	2.8 ± 0.0
Se <sub>SED</sub> (mg kg <sup>-1</sup> )	1.6 ± 0.05	0.33 ± 0.02	0.50 ± 0.04	0.14 ± 0.02	0.32 ± 0.02
Kd <sub>SED</sub>					
Depth	32,000	5900	11,000	7800	4800
Se <sub>water</sub> (%)	0.4 ± 0.0	1.4 ± 0.1	0.9 ± 0.2	1.3 ± 0.2	1.1 ± 0.0
Se <sub>phosphate</sub> (%)	4.7 ± 0.4	8.8 ± 0.6	10 ± 0.4	4.0 ± 0.5	8.4 ± 0.6
Se <sub>NaOH</sub> (%)	81 ± 2.0	59 ± 1.5	65 ± 1.2	16 ± 0.7	55 ± 2.2
Sed < 67 μm (%)	0.3	1.5	2.0	2.0	2.7
Sed 67–200 μm (%)	94	97	96	97	95
Sed > 200 μm (%)	5.8	1.5	1.6	0.7	2.5

Latitude (Lat) and Longitude (Long) expressed in decimal degrees, surface (surf.) and deep sampling (depth), water temperature (Temp), Oxygen (O<sub>2</sub>), Se in raw water (Se<sub>TOTAL</sub>; n = 5; mean ± SD), Se in filtered water with 0.22 μm membranes (Se < 0.22; n = 5; mean ± SD), and dissolved gaseous Se (Se<sub>G</sub>). Se in sediment (Se<sub>SED</sub>; n = 3; mean ± SD). Kd<sub>SED</sub>: distribution coefficients in sediment. Mean (n = 3) water-soluble fraction (Se<sub>water</sub>), exchangeable fraction (Se<sub>phosphate</sub>) and organic fraction (Se<sub>NaOH</sub>) of Se in sediment  
*bdl* below detection limit,  
*nd* not determined

decreases SPM. Optical properties of waters are mainly driven by dissolved organic carbon (DOC, in the range 4–18 mg L<sup>-1</sup>) and non-algal SPM concentrations (Laurion et al. 2010; Watanabe et al. 2011). When the ratio DOC/non-algal SPM increased, the optical appearance of the water changed from green to red, whereas it shifted from blue to yellow when it decreased. Beige colored waters contained the highest DOC concentrations, and concentrations decreased following the order brown, black and blue/green, and can correspond to pond ages. Based on field observations, NAS1A pond (white) is thus probably younger than KWAK1 (brown) and KWAK12 (black) ponds. However, the BGR-A (blue) pond is a newly-formed pond appeared less than 20 years ago (Calmels et al. 2008; Coulombe et al. 2016). Based on radiocarbon dating of sediments, Bouchard et al. (2011) estimated the formation of KWAK1 and KWAK12 thermokarst ponds at the end of the Little Ice Age (approx. 200–300 years ago). Other ponds surrounding these four thermokarst sites presented a strong degree of terrestrialization and the typical abundant vegetation of the forest-tundra zone in subarctic Québec (Payette and Bouchard, 2001). The catchment of SAS2A presented a clearly different state of permafrost degradation in evolving peatlands with an active layer depth of 60 cm (i.e. perennially frozen soil below 60 cm depth). SAS2A is probably the youngest pond, explaining why sediments consisted mainly of fibrous peat mixed with mineral matter (Table 1).

### Water and sediment monitoring

All materials (Teflon, Polyethylene) in contact with water samples were treated according to appropriate clean lab procedures. They were acid-washed, rinsed with ultrapure water (Milli-Q<sup>®</sup>), dried under a laminar flow hood and finally stored in sealed double polyethylene bags until use. All reagents were trace metal grade.

A sediment core (~ 20 cm length) was collected in each of the ponds KWAK2, KWAK6 and KWAK16 between 28th of June and 3rd of July 2007 with a percussion corer. Sampling and physicochemical properties of the sediment cores are detailed in Bouchard et al. (2011).

The other ponds were sampled on three consecutive days in August 2013. The surface sediments were collected with a gravity corer. The first two

centimeters of sediment were transferred to 60 ml polyethylene tubes and then freeze-dried. A portion of bulk sediment was stored for particle-size analysis determined by polydispersion and the rest was powdered and homogenized with a mortar and pestle made of agate and stored in sealed polypropylene (PP) recipients awaiting analysis.

Triplicates of representative sub-samples (250 mg) were digested in closed PP-tubes (DigiTUBEs, SCP Science) using 3.75 mL HCl (12 M) and 1.25 mL HNO<sub>3</sub> (14 M) heated at 80 °C for 2 h (Turner et al. 2013) using a temperature-controlled digestion system (DigiPREP MS, SCP Science). After being allowed to cool overnight, 1 mL of digested supernatant was transferred to 15 mL PE tubes and diluted with ultrapure water (Milli-Q water) for analysis. Reference sediment certified for Se concentration (BCR 227, Se: 2.04 ± 0.18 mg kg<sup>-1</sup>) was digested in triplicate and controls were performed in the absence of sediment. Accuracy was less than 4% from certified value and precision was 3% (RSD).

Selenium distribution in sediment was investigated by applying parallel single extractions and each extraction was performed in triplicate as described in Tolu et al. (2011). Briefly, ultrapure water, phosphate buffer (KH<sub>2</sub>PO<sub>4</sub>/K<sub>2</sub>HPO<sub>4</sub> 0.1 mol L<sup>-1</sup>) at pH 7 and NaOH 0.1 mol L<sup>-1</sup> isolated the bioavailable Se fraction (i.e. water soluble; Se<sub>water</sub>), the exchangeable Se fraction (i.e. adsorbed on particles; Se<sub>phosphate</sub>) and the fraction of Se associated with the organic matter (Se<sub>NaOH</sub>), respectively.

Mean concentrations of Se and standard deviation values are thus related to the variability associated to complete analysis of triplicates for each sediment sample.

Two water samples (5 L) were collected in both surface (down to 0.3 m depth) and bottom waters (up to 0.5 m above the bottom) with precaution to not modify the water stratification of the small observed ponds (10–20 m diameter) by using a non-metallic and PTFE coated sampler (5 L Go-Flo; General Oceanic). One liter of sample was immediately transferred into a Teflon bottle for subsequent purge and trap of the gaseous species. Additionally, 60 mL samples of water were collected in Teflon bottles and acidified with 150 µL HNO<sub>3</sub> (14 M) for total Se analyses (Se<sub>TOTAL</sub>). Total Se content in water was determined in unfiltered and filtered (0.22 µm) pond waters (10 mL) digested with HNO<sub>3</sub> (1 mL) and H<sub>2</sub>O<sub>2</sub>

(0.5 mL) in sealed tubes and incubated for 2 h at 90 °C in a hot block (DIGIPREP, SCP Science). Quality control and quality assurance of  $\text{Se}_{\text{TOTAL}}$  analyses were performed with TM-RAIN 04 certified water ( $\text{Se}$ :  $(0.84 \pm 0.27) \mu\text{g L}^{-1}$ ) and ARD-01 reference water ( $\text{Se}$ :  $86 \mu\text{g L}^{-1}$ ) diluted with ultrapure water by factors of 10 and 1000, respectively. The respective average deviation from the certified values were less than 1% and 9%, while obtained precision were 3% and 7% (% RSD), respectively.

Speciation analyses were done on samples immediately filtered through  $0.22 \mu\text{m}$  membrane filters (PTFE) and sampling bottles were filled to the top to avoid oxidation. All samples were stored in the dark at 4 °C until treatment and analysis. Suspended particulate matter concentrations were measured by filtration of up to 500 mL of sampled water on pre-weighed PVDF filters ( $< 0.45 \mu\text{m}$ ). Filters were then dried (50 °C) and weighed again. The natural partitioning of Se between particulate and dissolved phases was characterized by the partition coefficient,  $K_d$ , defined as the ratio of the particulate material Se concentration (in dry weight) to the dissolved Se concentration (Presser and Luoma 2010). This coefficient was calculated for sediment with the following equation:

$$K_{d_{\text{SED}}} = \frac{10^6 \text{Se}_{\text{SED}}}{\text{Se}_{<0.22}(\text{depth})} \quad (1)$$

with  $\text{Se}_{\text{SED}}$  expressed as  $\text{mg kg}^{-1}$ ,  $\text{Se}_{<0.22}$  expressed as  $\text{ng L}^{-1}$  and  $K_{d_{\text{SED}}}$  expressed in  $\text{L kg}^{-1}$  (Table 1).

#### Water incubation

The experiment was set up to understand the potential reactivity of thermokarst pond waters when simulating enhanced Se concentrations and biological activity. Water samples from SAS2A and KWAK1 ponds were collected in the oxygen depleted-hypolimnion where organic matter degradation by biotic and abiotic processes was expected to be the most important. Enriched isotope solutions of  $1000 \text{mg L}^{-1}$  were prepared from enriched elemental Se (Isoflex, Moscow, Russia) according to Van Dael et al. (2004). Incubations consisted in spiking  $1 \mu\text{g L}^{-1}$  of both isotopically stable enriched selenite ( $^{77}\text{SeO}_3^{2-}$ ; 98.3%  $^{77}\text{Se}$  and 1.7%  $^{78}\text{Se}$ ) and selenate ( $^{82}\text{SeO}_4^{2-}$ ; 99.2%  $^{82}\text{Se}$  and 0.8%  $^{80}\text{Se}$ ) species in raw bottom waters from SAS2A and KWAK1 ponds supplemented or not with

$5 \text{g L}^{-1}$  of wet local biofilms. The mixotrophic biofilms (i.e. periphyton) were sampled on subaquatic plants at SAS2A (50 cm depth) and on a net submerged at 1 m depth at KWAK1 above the oxycline depth (i.e.  $\text{O}_2 > 4 \text{mg L}^{-1}$ ). The biofilms that developed on artificial supports (AnoxKaldnes, Veolia Water Technology) submerged at 1 m depth in the studied zone were described by Rémy (2015). Close to the SAS2A pond, the SAS1A biofilm contained more than twice the KWAK1 biofilm content in organic matter (47% vs 20%, respectively), even though its cell density was two orders of magnitude lower ( $6.5 \cdot 10^7 \text{cell cm}^{-2}$ ) than in KWAK1 biofilm ( $6.3 \cdot 10^9 \text{cell cm}^{-2}$ , Rémy 2015). To limit any potential heterogeneity, incubations were conducted in triplicates and samples were analysed for dissolved ( $\text{Se}_{\text{SPE}}$ ) and gaseous ( $\text{Se}_{\text{G}}$ ) selenium speciation after spiking and after 72 h incubation. As water sample depth was below the maximum Secchi depth measured (Table 1) processes involved in situ do not include light induced processes. Consequently, to avoid photochemical pathways, all incubations were conducted in the dark at  $(15 \pm 1) \text{°C}$ . The duration of the experiment was chosen according to maximum volatilization rates determined by Zhang and Moore (1997). Total selenium analysis was performed on unfiltered and filtered ( $0.22 \mu\text{m}$ ) control and incubated samples. Results were expressed in % as the ratios of mean final concentration above mean initial concentration, i.e. mean concentration in 72 h incubated samples above mean concentration in control samples. Consequently, the error (%) was calculated as:

$$\text{error} = 100 \times \frac{x\sigma_y + y\sigma_x}{x^2} \quad (2)$$

with “ $x$ ” as the mean initial concentration ( $n = 3$ ), “ $y$ ” as the mean final concentration ( $n = 3$ ), “ $\sigma_x$ ” and “ $\sigma_y$ ” are the standard deviation associated with the means.

#### Analysis

##### Total selenium

Total Se was determined with an Agilent 7500ce ICP-MS instrument equipped with an octopole collision/reaction cell (C/RC). The sample introduction system consisted of a concentric nebulizer (Meinhard Associates, CA, USA) and a Scott double pass spray

chamber cooled to 2 °C. The C/RC was pressurized with helium and hydrogen of 99.995% purity (Air Liquide) delivered at 1 mL min<sup>-1</sup> and 4 mL min<sup>-1</sup>, respectively, in order to limit polyatomic interferences on Se isotopes and obtain accurate and precise determination of isotopic ratios (Tolu et al., 2014).

Four isotopes of Se (<sup>77</sup>Se, <sup>78</sup>Se, <sup>80</sup>Se and <sup>82</sup>Se) and two isotopes of Br (<sup>79</sup>Br and <sup>81</sup>Br) were analyzed in samples and Se and Br standard solutions to correct mathematically <sup>76</sup>Se<sup>1</sup>H<sup>+</sup>, <sup>77</sup>Se<sup>1</sup>H<sup>+</sup>, <sup>79</sup>Br<sup>1</sup>H<sup>+</sup> and <sup>81</sup>Br<sup>1</sup>H<sup>+</sup> interferences (Hinojosa Reyes et al. 2003; Tolu et al. 2014). Naturally present and tracer (<sup>77</sup>Se and <sup>82</sup>Se) Se concentrations were determined by reverse isotope dilution (RID), with natural abundance Se standard used as a spike, and <sup>78</sup>Se/<sup>77</sup>Se and <sup>80</sup>Se/<sup>82</sup>Se ratios selected as measured isotope pairs (Tolu et al. 2014).

#### *Water speciation of Se*

*Dissolved inorganic and organic Se species* Chromatographic separation of Se species was conducted using high performance liquid chromatography (Agilent 1100 series pump) coupled to ICP-MS. The separation was performed using Hypercarb column (10 cm × 4.6 mm i.d.; Thermo electron) and guard column with a formic acid mobile phase (240 mmol L<sup>-1</sup>, pH 2.4 adjusted with ammonia), delivered at 1 mL min<sup>-1</sup> flow allowing simultaneous separation of inorganic (selenite, selenate) and organic (trimethylselenonium ion, methane seleninic acid, selenomethionine, selenocystine) Se compounds (Dauthieu et al. 2006; Tolu et al. 2011). The injection volume was set at 100 µL. Species quantification was achieved by standard additions.

*Dissolved gaseous Se species* A purge and trap method was used for the pre-concentration of dissolved volatile Se compounds (Se<sub>G</sub>) with conservation of speciation. Briefly, Se<sub>G</sub> was removed from the water sample by purging with N<sub>2</sub> (30 L h<sup>-1</sup>) for 1 h. The resulting vapor went through a moisture trap maintained at - 20 °C to dry the vapor flux. The gas stream was then carried through a glass column filled with 1 cm<sup>3</sup> of activated charcoal. Following the purge, the glass columns were closed and stored in the dark at 4 °C in a sealed double bag until analysis (Alanoca et al. 2016; Bouchet et al.

2011). In the laboratory, separation and detection for the speciation of volatile selenium compounds consisted of the thermo-desorption of Se<sub>G</sub> on activated charcoal traps into a cryogenic trapping gas chromatography system hyphenated to an inductively coupled plasma mass spectrometer (CT-GC-ICPMS; e.g. Amouroux et al. 1998; Tessier et al. 2002). Blanks corresponded to a repeated treatment of water samples already degassed. The detection limit was 0.1 pg L<sup>-1</sup> when calculated from 5 blank signal backgrounds and was 0.5 pg L<sup>-1</sup> when calculated from 3 blank samples purged. The external calibration of CT-GC-ICPMS was realized by injection of a range of Se load from gravimetric working standard prepared from pure standard volatile dilutions of dimethyl selenide (DMSe; 99%) and dimethyl diselenide (DMDS<sub>2</sub>; 99%) purchased from Strem Chemicals. Mass concentrations of Se species were expressed as mass concentrations of Se throughout the text.

#### Gas exchange estimations

Gas exchanges across the air–water interface were calculated using the small lake gas exchange equation from Cole and Caraco (1998) based on total dissolved volatile Se (TVSe; Table 2; Amouroux and Donard 1997, Tessier et al. 2002) in surface samples and corresponding daily means of wind speed measured at 10 m height. Measured winds were representative of the mean wind speed of 5.6 m s<sup>-1</sup> calculated for the 1932–2000 period (Bhiry et al. 2011).

## Results and discussion

### Selenium distribution and speciation in thermokarst ponds

#### *Total Se in sediment*

Concentrations of Se in surface sediments of the thermokarstic ponds studied here ranged from (0.14 ± 0.02) mg kg<sup>-1</sup> to (1.60 ± 0.05) mg kg<sup>-1</sup> (mean ± SD; n = 3; Table 1). The major part of the Se<sub>SED</sub> variation was linked with particulate organic carbon content (R<sup>2</sup> = 0.98) comprised between 1 and 4% with a maximal concentration of 32% in SAS2A sediment. Such high concentrations have been related

**Table 2** Review of concentrations of total volatile Se (TVSe) and corresponding fractions of volatile Se species (DMSe, DMDSe), flux densities and annual fluxes to the atmosphere (Flux to atm)

Site	Description	Surf. (km <sup>2</sup> )	Se tot (μg L <sup>-1</sup> )	TVSe Water (pg L <sup>-1</sup> )	DMSe (%)	DMDSe (%)
<b>Lake and Wetland</b>						
Kuujuarapik, Québec, Canada	Arctic Thaw ponds	200,000	0.035-0.063	1-32	96	4
Pantanal Ponds, MS Brazil	Salt ponds	30,000		2- 66	92	8
Gola di Lago, Switzerland	Minerotrophic peatland		0.5-1.5	10	99,8-100	
Poopo Lake, Bolivia	Andean salt Lake	3191		1,038-1,740	60	37
Uru Uru Lake, Bolivia	Andean shallow Lake	214		42-1,679	49	41
Great Salt Lake, UT, USA	Salt Lake	1875	0.5	40-22,700		
Tulare Lake, San Joaquin Valley, CA, USA	Irrigation Ponds	0,02		10,838-108,995	80	13
Kesterson reservoir, San Joaquin Valley, CA, USA	Evaporation ponds #8/#12	4.8	284/63-79	$34 \times 10^6 / (3.8-17) \times 10^6$	99,8	0.1-0.2
<b>Coastal Bay</b>						
Arcachon Bay	Coastal Lagoon	100		30-426	81	14
Norway	Trondheim Fjords	??		12-156	79	21
<b>Estuary and Sea</b>						
Seine	Estuary	300		317-4,855	94	4
Scheldt	Estuary	268		51-8,067	84	12
Rhine	Estuary	193		37-2,423	73	23
Gironde	Estuary	650		22-1,351	82	13
North Atlantic	Ocean	41,490,000		37-417	44	56
East_ Mediterranean Sea	Ocean	2,500,000		20-75	64	36
Site	TVSe Air (pg L <sup>-1</sup> )	DMSe (%)	DMDSe (%)	Flux density ng (Se) (m <sup>-2</sup> day <sup>-1</sup> )	Flux to atm (ton year <sup>-1</sup> )	References
<b>Lake and Wetland</b>						
Kuujuarapik, Québec, Canada	No data			1-97 <sup>a</sup>	0.07-7.1	This study
Pantanal Ponds, MS Brazil	< 0.04			2-46 <sup>a</sup>	0.02-0.5	Tessier and Amouroux, Unpublished
Gola di Lago, Switzerland	No data			190-210		Vriens et al. (2014)
Poopo Lake, Bolivia	No data			481-868 <sup>a</sup>	0.6-1.0	Tessier and Amouroux, Unpublished
Uru Uru Lake, Bolivia	No data			25-1 588 <sup>a</sup>	0.002-0.12	Tessier and Amouroux, Unpublished
Great Salt Lake, UT, USA	No data			818-5,524 <sup>b</sup> ; 1,198-7,965 <sup>d</sup>	0.6-5.5	Diaz et al. (2009)
Tulare Lake, San Joaquin Valley, CA, USA	0.09-6.47	86	8	6,690-154,200 <sup>a</sup>	< 0.0011	Tessier and Amouroux, Unpublished

Table 2 continued

Site	TVSe Air ( $\mu\text{g L}^{-1}$ )	DMSe (%)	DMS <sub>2</sub> S (%)	DMDSe (%)	Flux density ng (Se) ( $\text{m}^{-2} \text{day}^{-1}$ )	Flux to atm ( $\text{ton year}^{-1}$ )	References
Kesterson reservoir, San Joaquin Valley, CA, USA	No data				$0.52\text{--}5.2 \times 10^{6\text{e}}$	0.9–9.1	Cook and Brutland (1987)
Coastal Bay							
Arcachon Bay	< 0.04				33–1751 <sup>c</sup>	0.001–0.06	Tessier and Amouroux, Unpublished
Norway	0.01–1.02	39	61	n.d.	9–471 <sup>c</sup>		Tessier and Amouroux, Unpublished
Estuary and Sea							
Seine	0.20–0.77	n.d.	78	22	150–2943 <sup>d</sup>	0.02–0.32	Tessier and Amouroux, Unpublished
Scheldt	0.04–0.08	100	n.d.	n.d.	75–14,752 <sup>d</sup>	0.007–1.4	Tessier et al. (2002)
Rhine	< 0.04				25–2140 <sup>d</sup>	0.002–0.15	Tessier et al. (2002)
Gironde	0.37–0.87	100	n.d.	n.d.	34–3911 <sup>d</sup>	0.008–0.93	Tessier et al. (2002) and Amouroux and Donard (1997)
North Atlantic	no data				111–1413 <sup>b</sup>	1,700–21,000	Amouroux et al. (2001)
East. Mediterranean Sea	0.07–0.16	60	40	n.d.	2–228 <sup>b</sup>	1.8–210	Amouroux and Donard (1996)

Fluxes are based on TVSe concentrations

n.d. not detected; SW: Surface Water

<sup>a</sup>Cole and Caraco (1998)<sup>b</sup>Liss and Merlivat (1986)<sup>c</sup>Borges (2004)<sup>d</sup>Clark et al. (1995)<sup>e</sup>Liss and Slater (1974)

to anthropogenic Se sources in the United Kingdom (Bryan and Langston 1992; Turner 2013), yet similar concentration ranges occurred naturally in seleniferous Cretaceous marine sedimentary rocks of the Canadian prairies (“the Northern Great Plains”; Dunn 1990) where Se concentrations in surface soils (< 2 mm) commonly ranged from 0.1 to 4.7 mg kg<sup>-1</sup> with a median value of 0.5 mg kg<sup>-1</sup> (Garrett et al. 2008) that defines seleniferous soils (Dhillon and Dhillon 2003).

In sediment cores collected from ponds KWAK2, KWAK6 and KWAK16, concentrations of Se were highest (0.17–0.30 mg kg<sup>-1</sup>) at the surface (< 1 cm depth) and decreased with depth to concentrations < 0.10 mg kg<sup>-1</sup> except in KWAK6 sediments (Fig. 2). In western Siberia lakes, accumulation of Se in surface sediment was induced by the coprecipitation of Se with colloidal Fe/Al oxy-hydroxides below the redox boundary as well as by organic matter complexation (Myneni et al. 1997; Pokrovsky et al. 2018).

#### *Labile selenium in surface sediment*

Single step extraction efficiencies to estimate the most mobile and bioavailable fraction (water-soluble fraction), the exchangeable fraction (phosphate buffer pH 7) and the organic fraction (alkaline extraction pH 13) of Se in sediments were in the range commonly observed in soils with 0.4–1.5%, 4.7–10% and 16–81% of Se<sub>SED</sub> extracted, respectively (Table 1; Coppin et al. 2006; Johnson et al. 2000; Séby et al. 1997; Sharmasarkar and Vance 1997; Tolu et al. 2011; Yamada and Hattori 1990). A positive relationship existed between particulate organic matter concentrations or the organic fraction of Se (Se<sub>NaOH</sub>) and Se concentration in the sediment (i.e., R<sup>2</sup> = 0.98 and R<sup>2</sup> = 0.56, respectively). Extreme values were represented by SAS2A and BGR-A ponds, which both significantly differ by their catchment vegetation and origin and show differences in chlorophyll *a* and dissolved organic carbon (SAS2A ≫ BGR-A; Crevecoeur et al. 2015). The SAS2A organic-rich sediment contained (32 ± 0.1) % of POC mainly represented by abundant root debris (> 200 μm = 5.8%) and plant fibers (Carex and Sphagnum). In this sediment, Se<sub>NaOH</sub> accounted for (81 ± 2.0) % while it was 16% of total Se in sediment of the mature BGR-A pond, in agreement with low organic carbon content (1.1% POC; Table 1). As a consequence, the

difference between Se accumulations in sediments was mainly related to the higher quantity of Se present in the estimated organic fraction. Consequently, incorporation and/or binding of Se with organic matter play a dominant role in the storage of Se in sediments of Canadian thermokarst ponds as observed in western Siberian lakes (Pokrovsky et al. 2018).

The residual fraction could be defined here as the difference between total Se in sediment (Se<sub>SED</sub>) and organic Se (Se<sub>NaOH</sub>). In contrast to the organic fraction, the residual fraction varied from 19% (SAS2A) to 84% (BGR-A). However, KWAK1, KWAK12, BGR-A and NAS1A showed similar concentrations of Se in the estimated residual fractions as 0.14, 0.17, 0.12 and 0.14 mg kg<sup>-1</sup>, respectively. The local Se background can thus be estimated as 0.1 mg kg<sup>-1</sup>.

#### *Water column*

All ponds exhibited strongly stratified shallow waters at the time of sampling (August 2013) with an oxic epilimnion from the surface (> 6.4 mg L<sup>-1</sup>) to about 1 m depth and an oxygen-depleted hypolimnion (< 0.6 mg L<sup>-1</sup>; Table 1). Bottom waters collected for monitoring and incubations were all anoxic. Sampling conditions were representative of the persistent thermal stratification and the presence of an anoxic/hypoxic layer at the bottom commonly observed on a yearly scale during summer and winter (Laurion et al. 2010). Total Se concentrations in bulk water (Se<sub>TOTAL</sub>) ranged from 18 to 107 ng L<sup>-1</sup>, and no clear difference existed between anoxic bottom waters and oxic surface waters except in pond NAS1A (Table 1). The 20% increase of Se<sub>TOTAL</sub> in NAS1A bottom waters corresponded to a 30% SPM increase, while dissolved Se concentrations (Se<sub><0.22</sub>) in bottom and surface filtered waters were not significantly different. As Se is mainly released during thawing of frozen peat, the higher temperature in summer and consequently deeper active layer boundary as well as decreasing water volume in ponds (i.e. evaporation), can result in maximal Se concentrations during summer season (Pokrovsky et al. 2018). Thus, the dissolved Se concentrations that ranged from (18 ± 7) to (67 ± 18) ng L<sup>-1</sup>, could be considered the highest annual concentrations. These concentrations were below the freshwater wildlife protection criterion (1 μg L<sup>-1</sup>) set by Environment Canada and the U.S.

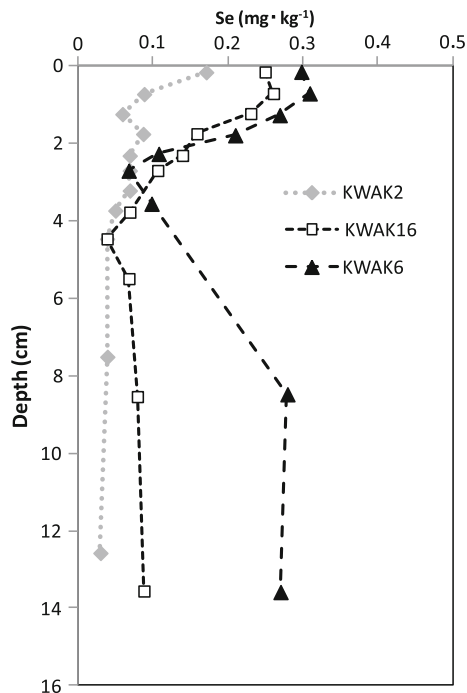


**Fig. 2** Selenium concentration vs depth for the sediment cores from ponds KWAK2, KWAK6 and KWAK16

Environmental Protection Agency as aquatic life water quality criterion ( $5 \mu\text{g L}^{-1}$ ) as well as below the limit of contaminated water set at  $200 \text{ ng L}^{-1}$  (USEPA 2002). Similar  $\text{Se}_{<0.22}$  concentrations were measured in 111 thermokast lakes across sporadic, discontinuous and continuous regions in western Siberia lowland ( $12\text{--}311 \text{ ng L}^{-1}$ ; Pokrovsky et al. 2018). These concentrations were linearly related to dissolved organic carbon (DOC) concentrations. In the present study, similar relation of selenium and organic carbon is observed in sediments. In August 2012, DOC concentrations were measured at  $3.5$ ,  $12$  and  $15 \text{ mg L}^{-1}$  in BGR-A, KWAK1 and SAS2A waters, respectively (Crevecoeur et al. 2015). Lower concentrations of both DOC and  $\text{Se}_{<0.22}$  in BGR-A compared to other ponds agreed with previous observation on the control of Se concentrations by variation in organic carbon concentrations (Pokrovsky et al. 2018).

During the sampling period, the only detectable dissolved gaseous Se compound was DMSe. All sampled ponds except NAS1A showed DMSe concentrations in the range  $< 0.17$  (LOD)– $4.1 \text{ pg L}^{-1}$  with no clear difference in DMSe concentrations between ponds or between surface and deep waters (i.e. oxic and anoxic

waters). In contrast, DMSe concentrations in the NAS1A pond were one order of magnitude higher than in other ponds, with the highest concentration in bottom waters ( $56 \text{ pg L}^{-1}$ ) as compared to surface waters ( $31 \text{ pg L}^{-1}$ ; Table 1). Observed differences between surface and bottom dissolved gaseous Se concentrations in NAS1A imply the formation of DMSe in depth as observed for  $\text{CO}_2$  and  $\text{CH}_4$  during stratification periods (Laurion et al. 2010), or simply be related to the volatilization of gaseous Se in the surface layer (i.e. considering photodegradation to be negligible due to low light penetration). Enhanced methylation of mercury was also noticed by Rémy (2015) with 56% of the present dissolved mercury in the form of methylmercury in the pond NAS1A as compared to 5.2% to 13% in the other ponds. The particularities of the NAS1A water were i) the high SPM load at the time of sampling with concentrations of  $470 \text{ mg L}^{-1}$  in surface and  $600 \text{ mg L}^{-1}$  in bottom waters, (Table 1), ii) the location of the pond at the limit of discontinuous permafrost zone (Fig. 1) and iii) the beige colored water usually presenting high DOC concentrations (Watanabee et al. 2011). Surfaces and heat absorption provided by high loads of suspended fine particles contribute to increase bacterial density. In other system such as estuaries, high turbidity zones presented an intense heterotrophic activity leading to carbon mineralization and biogas production and consequently produced significant amounts of volatile Se compounds (Amouroux and Donard 1997; Tessier et al. 2002). Despite high SPM concentration in NAS1A, the bacterial density at 1 m depth [ $(8.1 \pm 1.7) \times 10^6 \text{ cell mL}^{-1}$ ] was in the range of other investigated ponds [ $(3.7 \pm 0.7) \times 10^6 \text{ cell mL}^{-1}$  to  $(1.4 \pm 0.3) \times 10^7 \text{ cell mL}^{-1}$ ; Rémy 2015]. However, significant differences in community composition, cellular growth rates and top-down trophic effects (e.g., bacterivory, viral lysis) can be observed between ponds within valleys or landscapes within different permafrost zones (i.e. discontinuous vs sporadic permafrost landscapes), separating bacterial density from bacterial activity (Comte et al. 2015; Deshpande et al. 2016). Because of an insufficient amount of light penetrating the water column, autotrophic activity and photochemical degradation are limited. Even if dead photosynthetic organisms provided carbon sources for heterotrophic bacteria in all sampling sites, a particularity in amount or nature of nutrients and carbon released by peatland soils in

the catchment of NAS1A ponds could be responsible for enhanced bacterial production (Deshpande et al. 2016). In summer, Siberian thaw lakes situated in the discontinuous permafrost zone, received more intense inputs of dissolved organic matter and Se, both transported by the water flow in the active layer (i.e. over the permafrost boundary), compare to sporadic and continuous permafrost lakes (Pokrovsky et al. 2018). Clays preferentially adsorb aromatic dissolved organic carbon which increase bacterial production (Tietjen et al. 2005), and chromophoric dissolved organic matter (cDOM) play a major role in Se binding in thaw lake and its storage (Pokrovsky et al. 2018). Following photochemical decomposition of cDOM and DOC, smaller organic compounds in surface (Tietjen et al. 2005) can also participate to Se cycle and Se availability to bacteria mediated transformation. The particular geographical position of NAS1A compare to other ponds could indicate a higher reactivity of Se in discontinuous permafrost landscapes where nature and concentration of dissolved organic matter as carbon source and binding sites could affect bacterial communities and enhanced the activity of bacteria responsible for the biotransformation of Se into volatile Se species.

## Insights into selenium aquatic biogeochemistry

### *Reactivity in the aqueous phase*

The natural partitioning of Se in sediment ( $K_{dSED}$ ) in thermokarst ponds varied between 4800 (NAS1A) and 11,000 L kg<sup>-1</sup> (KWAK12) with an exceptionally high value in SAS2A (32,000 L kg<sup>-1</sup>; Table 1). This range of values was similar to that observed in a coastal wetland ( $K_{dSED}$ : 6500 L kg<sup>-1</sup>, Great Marsh coastal wetland, Delaware, USA; Presser and Luoma 2010; Velinsky and Cutter 1991) and was clearly higher than values commonly observed in rivers, lakes and reservoirs (100 <  $K_{dSED}$  < 5000; Presser and Luoma 2010). As expected, the negative linear relationship ( $R^2 = 0.84$ ;  $n = 5$ ) between  $K_{dSED}$  and the water soluble fraction of Se in sediment ( $Se_{bioavailable}$ ; Table 1) suggests a removal of  $Se_{SED}$  to the water column. Reducing conditions and high organic content can enhance Se transformation into insoluble inorganic Se species (e.g. coprecipitation of Se with colloidal Fe/Al oxy-hydroxides in oxygen depleted hypolimnion or reduction to elemental Se), and

together with Se accumulation in vegetal debris mediated by rhizospheric bacteria (de Souza et al. 1999), could explain the importance of the particulate phase and organic matter control on Se distribution.

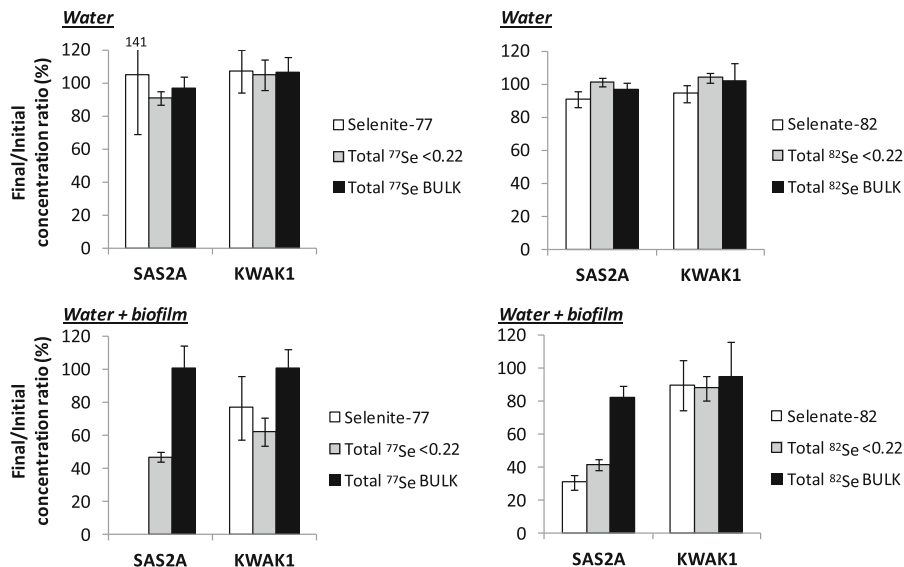
To understand the role of thermokarst pond waters in the cycling of potential atmospheric inputs of Se, bulk bottom waters from SAS2A and KWAK1 ponds were enriched with dissolved Se species (selenite-77 and selenate-82) and incubated in the dark for 24 h at 15 °C. In both pond waters, no clear decrease in the dissolved concentration of selenite-77 (<sup>77</sup>Se) nor selenate-82 (<sup>82</sup>Se) was observed at the end of the 72 h incubation time. Similarly, no trend appeared in the measurements of the isotope <sup>77</sup>Se in the dissolved (<sup>77</sup>Se<sub><0.22</sub>) or bulk (<sup>77</sup>Se<sub>BULK</sub>) waters, nor for the isotope <sup>82</sup>Se. Thus, the transfer of selenite-77 or selenite-82 tracers to the particulate phase or transformation into other Se species was negligible under our experimental conditions (Fig. 3).

However, when in situ periphytic biofilm was added to pond waters, selenite-77 and selenate-82 decreased by 100% and 69%, respectively, during the incubation time in SAS2A, while no clear trend was observed in KWAK1.

At the end of the experiment in SAS2A, dissolved concentrations of <sup>77</sup>Se and <sup>82</sup>Se (Total <sup>77</sup>Se<sub><0.22</sub> and Total <sup>82</sup>Se<sub><0.22</sub>) were 50% of corresponding concentrations in bulk waters. Half of initially added selenite-77 was associated to the particulate phase by adsorption/absorption processes on biofilm and related extracellular particulate organic matter. As no selenite-77 was detected in the dissolved phase, dissolved concentrations of <sup>77</sup>Se (Total <sup>77</sup>Se<sub><0.22</sub>) was related to the transformation of selenite-77 into other chemical forms of dissolved <sup>77</sup>Se undetected by chromatographic separation method.

On the contrary, no transformation of selenate was observed as concentrations of dissolved selenate-82 corresponded to the Total <sup>82</sup>Se<sub><0.22</sub> measured. Consequently, only adsorption/absorption on particulate biofilm material and/or biofilm occurs for 69% of selenate-82. The difference between selenite and selenate can be related to the higher affinity of selenite for organic matter binding sites (Gustafsson and Johnsson 1994) and its higher bioavailability (Besser et al. 1993; Luoma and Rainbow, 2008) as compared to selenate. Internalization of selenate and selenite in algae occurs via distinct pathways and is more rapid for the later (e.g. Vriens et al. 2016). The absence of

**Fig. 3** Isotopic concentrations of Se and Se in filtered ( $< 0.22 \mu\text{m}$ ) and bulk waters 3 days after selenite-77 and selenate-82 enrichment of bulk waters from ponds SAS2A and KWAK1 with and without biofilm enrichment. Ratios of mean final concentration above mean initial concentration ( $n = 3$ ) are expressed in %. Error bars were calculated according to the formula detailed in the Materials and methods section



Se-containing peaks during chromatographic analysis of the dissolved phase indicated that newly-formed dissolved Se species were not eluted under the conditions used and were thus different from commercially available Se standards (i.e., selenite, selenate, trimethylselenonium ion, selenomethionine, selenocystine, selenoethionine and methane seleninic acid; Dauthieu et al. 2006; Tolu et al. 2011). Similarly, laboratory algal cultures exposed to selenate at higher concentration levels ( $10$  to  $25 \mu\text{g L}^{-1}$ ) have shown organic Se metabolites release including several unidentified organic Se species, such as cyclic structures derived from selenomethionine and selenomethionine-Se-oxide (LeBlanc and Wallschläger 2016). Vriens et al. (2016) showed that intracellular Se speciation in a freshwater algae exposed to Se [IV] and Se [IV] changed depending of the exposure concentrations. In the present study, experimental exposure with compound specific enriched stables isotopes allowed assessment of Se reactivity at much lower Se concentration (below  $1 \mu\text{g L}^{-1}$  or  $1.25 \cdot 10^{-2} \mu\text{M}$ ), that was 2400 to 6000 times lower than the range of concentrations ( $30 \mu\text{M}$  and  $75 \mu\text{M}$ ) that were demonstrated to affect intracellular Se speciation in such model algae (Vriens et al. 2016).

The release of dissolved organic carbon and chromophoric dissolved organic matter together with the presence of less soluble and labile elements (Al, Fe) can also lead to Se storage in the form of organic aromatic-rich complexes and organo-mineral colloids (Pokrovsky et al. 2018). Differences in chlorophyll-a

concentrations existed between ponds (SAS2A  $>$  BGR-A; Crevecoeur et al. 2015), but because incubation occurred in the dark and oxygen depleted waters, metabolic processes involved in inorganic Se biotransformation could also imply the respiration of selenium oxyanions (i.e. selenite and selenate reduction) by anoxygenic microorganisms. Such Se biotransformation pathways are known to potentially induce the formation of insoluble metal selenide or extracellular nanospheres of amorphous Se (Oremland et al. 1989, 2004; Vriens et al. 2016), that cannot be detected using dissolved compounds speciation analysis.

The microbial composition of in situ biofilms in SAS2A and KWAK1 was not investigated. Nevertheless, despite a similarity of thaw pond bacterial communities at the regional scale (Actinobacteria and beta-proteobacteria), more divergent communities occurred within ponds of a same valley as a consequence of the variability in carbon and nutrient inputs, dissolved oxygen levels and bacterivores among the ponds as reported in Rossi et al. (2013) and Comte et al. (2015). This difference could explain the contrasting response in inorganic Se biotransformation between SAS2A and KWAK1 ponds.

#### Formation of gaseous Se species

The net formation rate of gaseous Se species was quantified as  $\text{DM}^{77}\text{Se}$  and  $\text{DMD}^{77}\text{Se}$  originating from selenite-77 transformation, and  $\text{DM}^{82}\text{Se}$  and

DMD<sup>82</sup>Se from selenate-82. In incubated waters, mean concentrations of formed DMSe were similar between KWAK1 and SAS2A waters (3.4–5.2 pg L<sup>-1</sup>) and equally formed from selenite-77 or selenate-82. The mean production rates of DMSe accounted for  $(1.5 \pm 0.3) \times 10^{-6} \text{ day}^{-1}$  of the initially added amount of selenite-77, and for  $(1.4 \pm 0.5) \times 10^{-6} \text{ day}^{-1}$  of the amount of selenate-82 when including both KWAK1 and SAS2A waters. No DMDSe could be detected during the experiment.

Enrichment with in situ biofilm increased DMSe concentrations by a factor of 18–30 for KWAK1 and 38–76 for SAS2A. The mean rate of DMSe production from selenite-77 or selenate-82 was  $(3.6 \pm 0.9) \times 10^{-5} \text{ day}^{-1}$  in KWAK1 samples and  $(9.1 \pm 6.5) \times 10^{-5} \text{ day}^{-1}$  in SAS2A samples. Mean concentrations of DMDSe were two orders of magnitude lower than those of DMSe in both biofilm supplemented waters (1.0 – 2.6 pg L<sup>-1</sup>) with a global production rate of  $(5.5 \pm 4.4) 10^{-7} \text{ day}^{-1}$ . A strong and positive relationship existed between the production of DM<sup>77</sup>Se and DM<sup>82</sup>Se in both KWAK1 ( $R^2 = 0.98$ ;  $n = 3$ ) and SAS2A ( $R^2 = 0.99$ ;  $n = 3$ ) waters. Mean ratios between DM<sup>77</sup>Se and DM<sup>82</sup>Se production rates were  $1.4 \pm 0.1$  and  $2.7 \pm 0.2$  ( $n = 3$ , mean  $\pm$  SD) for KWAK1 and SAS2A, respectively, indicating that a larger amount of DMSe was produced from selenite-77 rather than from selenate-82 in both waters.

Because no transformation of inorganic Se was observed in KWAK1 waters, and no particular chemical form of dissolved Se in SAS2A was elucidated, it was not possible to identify neither intermediate organic Se species at the origin of volatile Se (Besser et al. 1989; Cooke and Bruland 1987), nor those that could promote their formation through heterotrophic degradation of complex Se compounds or through autotrophic transformation (Amouroux et al. 2000; Luxem et al. 2017). The observed concentrations of natural dissolved DMSe in waters (i.e. SAS2A = 3.1 pg L<sup>-1</sup>; KWAK1 = 1.7 pg L<sup>-1</sup>) were respectively 31 and 11 times higher than the estimated daily production from the experimental production rate applied to Se<sub>TOTAL</sub> in SAS2A and KWAK1 waters. As determined from the experimental data, the role of in situ biofilms in promoting DMSe formation can be significant and may display strong seasonal variation during ice melt and water runoff events, as well as the

potential for volatile Se production in combination with photosynthesis (e.g. Luxem et al. 2017). However, the observed higher DMSe concentrations in the water column can also be related to the potential accumulation and slow turnover of the produced DMSe in such natural waters and/or to additional inputs from surface sediments (i.e., Ellwood et al. 2015; Tessier et al. 2002; Zhang and Moore 1997).

Biogeochemical implications for Se evasion and accumulation

#### *Se volatilization to the atmosphere*

Se flux densities estimated from small lake gas exchange equation and volatile Se concentrations in surface water, were in the range 1–97 ng m<sup>-2</sup> day<sup>-1</sup> (Table 2). Even if particular processes occurring in sampled thermokarst ponds participate in Se cycle and can be briefly resumed in (i) pronounced hypoxia in the hypolimnion and (ii) a clear capacity of local biofilms to transform dissolved inorganic Se into volatile Se species, total dissolved volatile Se concentrations and outgassing rates of volatile Se toward the atmosphere were lower or similar to minimum flux densities measured in peatlands in southern Switzerland, in major European estuaries, in the North Atlantic Ocean and the eastern Mediterranean Sea (Table 2). Surprisingly, emission rates of subarctic thermokarst ponds and aquatic systems of the Pantanal region ( $2\text{--}46 \text{ ng Se m}^{-2} \text{ day}^{-1}$ ), the world's largest tropical wetland located in the center of South America, were comparably low.

Nevertheless, the high total surface area occupied by these abundant thermokarst ponds in northern Canada may induce significant yearly emissions of Se to the atmosphere, probably in the order of a thousand kg of Se per year, a value that may exceed some of the aquatic system emissions reported in Table 2, with the exception of particular water bodies such as the Great Salt Lake ( $0.6\text{--}5.5 \text{ tons year}^{-1}$ ) and the Kesterson reservoir ( $0.9\text{--}9.1 \text{ tons year}^{-1}$ ), as well as larger marine ecosystems like the Mediterranean Sea ( $1.8\text{--}210 \text{ tons year}^{-1}$ ) and the North Atlantic Ocean ( $1700\text{--}21,000 \text{ tons year}^{-1}$ ). Because our data only represent a first estimate of Se emissions from this particular type of aquatic media, the extrapolation of yearly fluxes and fluxes from local data to a larger geographic area should be considered with caution

(e.g. effect of the ice cover and thawing). However, these results clearly showed that Canadian thaw lakes are among the major production zones of volatile Se and, together with Siberian thaw lakes (Pokrovski et al. 2018), have to be considered to assess the Se cycle at a global scale.

Forecasting Se fluxes with the possible broad-scale response of thermokarst pond and the extent of thawing permafrost is challenging as numerous factors are involved in Se cycling in these rapidly changing environments. The temporal evolution of thermokarst ponds since their inception, including settling of mineral particles (clays and silts) and the development of terrestrial vegetation in the surrounding catchment, may result in strong variations in the limnological conditions of nearby ponds (Bouchard et al. 2011; Calmels et al. 2008; Payette et al. 2004; Pienitz et al. 2008; Watanabe et al. 2011) and impact Se reactivity. Changes in organic matter content and redox conditions over the year (seasonal effects) and also over the permafrost degradation period may differently affect factors controlling Se solubility and deposition by biotic (i.e. anaerobic bacteria) and abiotic (i.e. Fe/Mn oxides) processes (Balistrieri and Chao 1990; Belzile et al. 2000; Garbisu et al. 1996; Masscheleyn et al. 1990; Oremland et al. 1989; Stolz et al. 2006; Zhang and Moore 1997). The rapid attenuation of light penetration and the strong stratification of dissolved O<sub>2</sub> concentrations in the water column also strongly reduce light photodegradation of volatile Se compounds (Mason et al., 2018) and favor specific bacterial assemblages (Laurion et al. 2010; Rossi et al. 2013), potentially involved in Se reduction and methylation. The duration of ice cover varies with latitude and may limit exchanges of Se with the atmosphere. Moreover, bi-annual and punctual (i.e. windy periods) mixing periods could greatly increase Se recycling by favoring mobile forms of Se (e.g. selenate) under oxic conditions and enhance sediment–water–atmosphere exchanges (e.g. Velinsky and Cutter 1991).

#### *Accumulation of Se in sediments*

Sediment cores collected in 2011 (0–20 cm depth, subsampled at 0.5 cm resolution, i.e. present-day to ~ 7000 year BP; Bouchard et al. 2011) in three ponds located at the KWAK site revealed minimum Se concentrations of 0.05 mg kg<sup>-1</sup> at 3 cm depth (year

1963) with an enrichment of Se concentration independent of grain size to 0.2–0.3 mg kg<sup>-1</sup> at the surface (Fig. 2). The local background concentration of Se in sediment was then estimated between 0.05 mg kg<sup>-1</sup> and 0.10 mg kg<sup>-1</sup> (i.e. the estimated residual fractions of Se in surface sediments). Daily sedimentation rates can show a great seasonal variability (e.g., 0.2–5.5 mm day<sup>-1</sup> in BGR1; Coulombe et al. 2016) but can be estimated on a yearly basis. Sedimentation rates in KWAK1 yielded a mean mass accumulation of 400 g m<sup>-2</sup> year<sup>-1</sup> (Bouchard et al. 2011), the estimated local background allowed to calculate a rate of Se transfer in the sediment in the range of 0.02 mg m<sup>-2</sup> year<sup>-1</sup> to 0.04 mg m<sup>-2</sup> year<sup>-1</sup>.

In surface sediments sampled in 2013, Se was associated at 59% with the estimated organic fraction of KWAK1 sediment. The distribution of Se in core sediments from KWAK2, KWAK6 and KWAK16 could then be due to the presence of Se associated to organic matter freshly deposited at the surface and diagenetic processes affecting organic matter at depth. Recycling of organic Se complexes by the diagenesis (i.e. in reducing conditions) are known to favor the formation of insoluble elemental Se and/or metal selenides and Se-containing minerals (Masscheleyn and Patrick Jr 1993; Zhang and Moore 1997). However, no strong accumulation of Se at depth corresponding to pond inception (i.e., maximum organic matter content) was observed in thermokarst ponds. Consequently, a recycling of Se associated with the organic matter and the release to the water column occurred also and could be associated with mixing events within the water column.

#### **Conclusion**

In the context of steadily increasing Se emissions from human activities at a global scale (Mason et al. 2018), especially those related to coal mining activities, as well as rapid permafrost thaw due to climate warming, an innovative approach based on incubation of thermokarst lake waters with stable isotopically enriched selenite and selenate at relevant environmental concentrations (1 µg L<sup>-1</sup>) allowed to simulate and trace inorganic Se transformation after wet deposition and highlighted the role of biofilms in Se cycling.

Results confirmed the absence of heterotrophic transformation of Se in waters as observed in western Siberian thaw lakes (Pokrovsky et al. 2018), but highlighted the role of particular biofilms (microbial and algal species) in Se biotransformation and its potential contribution for the formation of insoluble inorganic Se species and Se storage in sediments.

The volatilization rate of Se measured in summer corresponded to low flux densities that are comparable to other continental aquatic systems. In the context of accelerated permafrost thaw, a better understanding of the early developmental stages of thermokarst ponds located on organic-rich soils (i.e. peatland) and of Se reactivity during transition periods (e.g. first day after ice covered period) and mixing events are of great interest to further specify Se budgets.

**Acknowledgements** We thank Claude Tremblay, Najat Bhiri and Warwick F. Vincent for their support at the field station of Centre for Northern Studies (CEN); Michel Cremer for particle-size distribution analyses; Laura Forsström for support in physico-chemical measures; the TAKUVIK research program and the Arctic Metals project (ANR-11-CESA-0011) for logistic and financial support; posthumously, Jean Carignan, at the origin of the project Arctic Metals.

## References

- ACIA (2004) Impacts of a warming Arctic: Arctic climate impact assessment, overview report. Cambridge University Press, Cambridge
- Alanoca L, Amouroux D, Monperrus M, Tessier E, Goni M, Guyoneaud R, Acha D, Gassie C, Audry S, Garcia ME, Quintanilla J, Point D (2016) Diurnal variability and biogeochemical reactivity of mercury species in an extreme high altitude lake ecosystem of the Bolivian Altiplano. *Environ Sci Pollut Res* 23:6919–6933
- Allard M, Seguin MK (1987) The Holocene evolution of permafrost near the tree line, on the eastern coast of Hudson Bay (northern Quebec). *Can J Earth Sci* 24:2206–2222
- Amouroux D, Donard OFX (1996) Maritime emission of selenium to the atmosphere in Eastern Mediterranean seas. *Geophys Res Lett* 23(14):1777–1780
- Amouroux D, Donard OFX (1997) Evasion of selenium to the atmosphere via biomethylation processes in the Gironde estuary, France. *Mar Chem* 58:173–188
- Amouroux D, Tessier E, Péchéryan C, Donard OFX (1998) Sampling and probing volatile metal(loid) species in natural waters by in situ purge and cryogenic trapping followed by gas chromatography and inductively coupled plasma mass spectrometry (P-CT-GC-ICP/MS). *Anal Chim Acta* 377:241–254
- Amouroux D, Péchéryan C, Donard OFX (2000) Formation of volatile selenium species in synthetic seawater under light and dark experimental conditions. *Appl Organomet Chem* 14:236–244
- Amouroux D, Liss PS, Tessier E, Hamren-Larsson M, Donard OFX (2001) Role of oceans as biogenic sources of selenium. *Earth Planet Sci Lett* 189:277–283
- Balistrieri LS, Chao TT (1990) Adsorption of selenium by amorphous iron oxyhydroxide and manganese dioxide. *Geochim Cosmochim Acta* 54:739–751
- Beavington F, Cawse PA, Wakenshaw A (2004) Comparative studies of atmospheric trace elements: improvements in air quality near a copper smelter. *Sci Total Environ* 332:39–49
- Belzile N, Chen YW, Xu R (2000) Early diagenetic behavior of selenium in freshwater sediments. *Appl Geochem* 15:1439–1454
- Bennett JP (1995) Abnormal chemical element concentrations in lichens of Isle Royale National Park. *Environ Exp Bot* 35:259–277
- Besser JM, Huckins JN, Little EE, La Point TW (1989) Distribution and bioaccumulation of selenium in aquatic microcosms. *Environ Pollut* 62:1–12
- Besser JM, Canfield TJ, Lapoint TW (1993) Bioaccumulation of organic and inorganic selenium in a laboratory food-chain. *Environ Toxicol Chem* 12:57–72
- Bhiri N, Delwaide A, Allard M, Bégin Y, Filion L, Lavoie M, Nozais C, Payette S, Pienitz R, Saulnier-Talbot É, Vincent WF (2011) Environmental change in the Great Whale River region, Hudson Bay: five decades of multidisciplinary research by centre d'études Nordiques (CEN). *Ecoscience* 18:182–203
- Blazina T, Läderach A, Jones GD, Sodemann H, Wernli H, Kirchner JW, Winkel LHE (2017) *Environ Sci Technol* 51:108–118
- Borges AV, Delille B, Schiettecatte LS, Gazeau F, Abril G, Frankignoulle M (2004) Gas transfer velocities of CO<sub>2</sub> in three European estuaries (Randers Fjord, Scheldt, and Thames). *Limnol Oceanogr* 49:1630–1641
- Bouchard F, Francus P, Pienitz R, Laurion I (2011) Sedimentology and geochemistry of thermokarst ponds in discontinuous permafrost, subarctic Quebec, Canada. *J Geophys Res* 116:G00M04
- Bouchard F, Francus P, Pienitz R, Laurion I, Feyte S (2014) Subarctic thermokarst ponds: investigating recent landscape evolution and sediment dynamics in thawed permafrost of northern Québec (Canada). *Arct Antarct Alp Res* 46:251–271
- Bouchet S, Tessier E, Monperrus M, Bridou R, Clavier J, Thouzeau G, Amouroux D (2011) Measurements of gaseous mercury exchanges at the sediment–water, water–atmosphere and sediment–atmosphere interfaces of a tidal environment (Arcachon Bay, France). *J Environ Monit* 13:1351–1359
- Brown J, Ferrians OJ, Heginbottom JA, Melnikov ES (1998) Digital CircumArctic Map of Permafrost and Ground-Ice Conditions. In: International Permafrost Association, Data and Information Working Group, comp. Circumpolar Active Layer Permafrost System (CAPS), version 1.0. CD-ROM available from National Snow and Ice Data Center, nsidc@kryos.colorado.edu. NSIDC, University of Colorado, Boulder
- Bryan GW, Langston WJ (1992) Bioavailability, accumulation and effects of heavy metals in sediments with special

- reference to the United Kingdom estuaries: a review. *Environ Pollut* 76:89–131
- Calmels F, Allard M, Delisle G (2008) Development and decay of a lithalsa in Northern Québec: a geomorphological history. *Geomorphology* 97:287–299
- Carignan J, Gariépy C (1995) Isotopic composition of epiphytic lichens as a tracer of the sources of atmospheric lead emissions in southern Québec, Canada. *Geochim Cosmochim Acta* 59:4427–4433
- Clark JF, Schlosser P, Simpson HJ, Stute M, Wanninkhof R, Ho DT (1995) Relationship between gas transfer velocities and wind speeds in the tidal Hudson River determined by the dual tracer technique. In: Jähne B, Monahan EC (eds) *Air-Water Gas Transfer*. Hanau, Germany
- Cofala J, Amann M, Klimont Z, Kupiainen K, Höglund-Isaksson L (2007) Scenarios of global anthropogenic emissions of air pollutants and methane until 2030. *Atmos Environ* 41:8486–8499
- Cole JJ, Caraco NF (1998) Atmospheric exchange of carbon dioxide in a low-wind oligotrophic lake measured by the addition of SF<sub>6</sub>. *Limnol Oceanogr* 43:647–656
- Comte J, Monier A, Crevecoeur S, Lovejoy C, Vincent WF (2015) Microbial biogeography of permafrost thaw ponds across the changing northern landscape. *Ecography* 38:001–010
- Cooke TD, Bruland KW (1987) Aquatic chemistry of selenium: evidence of biomethylation. *Environ Sci Technol* 21:1214–1219
- Coppin F, Chabroulet C, Martin-Garin A, Balesdent J, Gaudet JP (2006) Methodological approach to assess the effect of soil ageing on selenium behaviour: first results concerning mobility and solid fractionation of selenium. *Biol Fertil Soils* 42:379–386
- Coulombe O, Bouchard F, Pienitz R (2016) Coupling of sedimentological and limnological dynamics in subarctic thermokarst ponds in Northern Québec (Canada) on an interannual basis. *Sediment Geol* 340:15–24
- Crevecoeur S, Vincent WF, Comte J, Lovejoy C (2015) Bacterial community structure across environmental gradients in permafrost thaw ponds: methanotroph-rich ecosystems. *Front Microbiol* 6:192
- Cutter GA, Church TM (1986) Selenium in western Atlantic precipitation. *Nature* 322:720–722
- Cutter GA, Cutter LS (2004) Selenium biogeochemistry in the San Francisco Bay estuary: changes in water column behavior. *Estuar Coast Shelf S* 61:463–476
- Dauthieu M, Bueno M, Darrouzes J, Gilon N, Potin-Gautier M (2006) Evaluation of porous graphitic carbon stationary phase for simultaneous preconcentration and separation of organic and inorganic selenium species in “clean” water systems. *J Chromatogr A* 1114:34–39
- de Souza MP, Huang CPA, Chee N, Terry N (1999) Rhizosphere bacteria enhance the accumulation of selenium and mercury in wetland plants. *Planta* 209:259–263
- Deshpande BN, Crevecoeur S, Matveev A, Vincent WF (2016) Bacterial production in subarctic peatland lakes enriched by thawing permafrost. *Biogeosciences* 13:4411–4427
- Dhillon KS, Dhillon SK (2003) Distribution and management of seleniferous soils. *Adv Agron* 79:119–184
- Dunn CE (1990) Lithochemical study of the Cretaceous in Central Saskatchewan—preliminary report. Miscellaneous report 90-4. Saskatchewan Geological Survey, Saskatchewan Energy and Mines
- Diaz X, Johnson WP, Oliver WA, Naftz DL (2009) Volatile selenium flux from the great salt lake. *Utah. Environ Sci Tech* 43(1):53–59
- Ellwood MJ, Schneider L, Potts J, Batley GE, Floyd J, Maher WA (2015) Volatile selenium fluxes from selenium-contaminated sediments in an Australian coastal lake. *Environ Chem* 13:68–75
- Garbisua C, Ishii T, Leighton T, Buchanan BB (1996) Bacterial reduction of selenite to elemental selenium. *Chem Geol* 132:199–204
- Garrett RG, Thorleifson LH, Matile G, Adcock SW (2008) Till geochemistry, mineralogy and lithology, and soil geochemistry—data from the 1991–1992 Prairie Kimberlite Study. Geological Survey of Canada Open File 5582
- Gustafsson JP, Johnsson L (1994) The association between selenium and humic substances in forested ecosystems—laboratory evidence. *Appl Organomet Chem* 8:141–147
- Hillaire-Marcel C (1976) La déglaciation et le relèvement isostatique sur la côte est de la baie d’Hudson. *Cahiers de géographie du Québec* 20:185–220
- Hinojosa Reyes L, Marchante-Gayón JM, García Alonso JI, Sanz-Medel A (2003) Determination of selenium in biological materials by isotope dilution analysis with an octopole reaction system ICP-MS. *J Anal Atom Spectrom* 18:11–16
- Johnson CC, Ge X, Green KA, Liu X (2000) Selenium distribution in the local environment of selected villages of the Keshan Disease belt, Zhangjiakou District, Hebei Province, People’s Republic of China. *Appl Geochem* 15:385–401
- Kagawa M, Ishizaka Y, Ohta K (2003) Sources of sulfate in winter aerosols over the Sea of Japan, as inferred from selenium composition. *Atmos Environ* 37:1593–1600
- Lag J, Steinnes E (1974) Soil selenium in relation to precipitation. *Ambio* 3:237–238
- Laurion I, Vincent WF, MacIntyre S, Retamal L, Dupont C, Francus P, Pienitz R (2010) Variability in greenhouse gas emissions from permafrost thaw ponds. *Limnol Oceanogr* 55:115–133
- LeBlanc KL, Wallschläger D (2016) Production and release of selenomethionine and related organic selenium species by microorganisms in natural and industrial waters. *Environ Sci Technol* 50:6164–6171
- Lemly AD (1994) Mining in northern Canada: expanding the industry while protecting arctic fishes—a review. *Ecotoxicol Environ Saf* 29:229–242
- Lemly AD (2004) Aquatic selenium pollution is a global environmental safety issue. *Ecotoxicol Environ Saf* 59:44–56
- Liss PS, Merlivat L (1986) In: Buat-Ménard P. (eds) *The role of air-sea exchange in geochemical cycling*. NATO ASI Series (Series C: Mathematical and Physical Sciences), vol 185. Springer, Dordrecht
- Liss PS, Slater PG (1974) Flux of Gases across the Air-Sea Interface. *Nature* 247:181–184
- Luoma S, Rainbow PS (eds) (2008) *Metal contamination in aquatic environments: science and lateral management*. Cambridge University Press, Cambridge
- Luxem KE, Vriens B, Behra R, Winkel LHE (2017) Studying selenium and sulfur volatilisation by marine algae

- Emiliania huxleyi* and *Thalassiosira oceanica* in culture. *Environl Chem* 14:199–206
- Maenhaut W, Cornille P, Pacyna JM, Vitols V (1989) Trace element composition and origin of the atmospheric aerosol in the Norwegian arctic. *Atmos Environ* 23:2551–2569
- Mason RP, Soerensen AL, DiMento BP, Balcom PH (2018) The global marine selenium cycle: insights from measurements and modeling. *Global Biogeochem Cy* 32:1720–1737
- Masscheleyn PH, Patrick WH Jr (1993) Biogeochemical processes affecting selenium cycling in wetlands. *Environ Toxicol Chem* 12:2235–2243
- Masscheleyn PH, Delaune RD, Patrick WH Jr (1990) Transformations of selenium as affected by sediment oxidation-reduction potential and pH. *Environ Sci Technol* 24:91–96
- Mosher BW, Duce RA (1987) A global atmospheric selenium budget. *J Geophys Res* 92:13289–13298
- Myneni SCB, Tokunaga TK, Brown GE (1997) Abiotic Selenium redox transformations in the presence of Fe (II, III) oxides. *Science* 278:1106–1109
- Nriagu JO (1989) A global assessment of natural sources of atmospheric trace metals. *Nature* 338:47–49
- Nriagu JO, Davidson CI (1986) *Toxic metals in the atmosphere*. Wiley, New York
- Nriagu JO, Pacina JM (1988) Quantitative assessment of worldwide contamination of air, water and soils by trace metals. *Nature* 333:134–139
- Oremland RS, Hollibaugh JT, Maest AS, Presser TS, Miller LG, Culbertson CW (1989) Selenate reduction to elemental selenium by anaerobic bacteria in sediments and culture: biogeochemical significance of a novel, sulfate-independent respiration. *Appl Environ Microbiol* 55:2333–2343
- Oremland RS, Herbel MJ, Switzer Blum J, Langley S, Beveridge TJ, Ajayan PM, Sutto T, Ellis AV, Curran S (2004) Structural and spectral features of selenium nanospheres produced by Se-respiring bacteria. *Appl Environ Microbiol* 70:52–60
- Pacyna JM, Pacyna EG (2001) An assessment of global and regional emissions of trace metals to the atmosphere from anthropogenic sources worldwide. *Environ Rev* 9:1–30
- Payette S, Bouchard A (2001) Le contexte physique et biogéographique. In: Payette S, Rochefort L (eds) *Écologie des tourbières du Québec-Labrador*. Les Presses de l'Université Laval, Québec
- Payette S, Rochefort L (eds) (2001) *Écologie des Tourbières du Québec-Labrador*. Presse de l'Université Laval, Québec
- Payette S, Delwaide A, Caccianiga M, Beauchemin M (2004) Accelerated thawing of subarctic peatland permafrost over the last 50 years. *Geophys Res Lett* 31:L18208
- Pienitz R, Doran P, Lamoureux S (2008) Origin and geomorphology of lakes in the polar regions. In: Vincent WF, Laybourn-Parry J (eds) *Polar Lakes and Rivers-Limnology of Arctic and Antarctic Aquatic Ecosystems*. Oxford University Press, Oxford
- Pokrovsky OS, Bueno M, Manasypov RM, Shirokova LS, Karlsson J, Amouroux D (2018) Dissolved organic matter controls seasonal and spatial selenium concentration variability in thaw lakes across a permafrost gradient. *Environ Sci Technol* 52:10254–10262
- Presser TS, Luoma SN (2010) A methodology for ecosystem-scale modeling of selenium. *Integr Environ Asses* 6:685–710
- Rémy PP (2015) Role of different microbial compartments (biofilms, suspended matters, surface sediment) and some of them components (bacterial cells, extracellular polymeric substances and biominerals) on HgII methylation and reduction. PhD thesis
- Riordan B, Verbyla D, McGuire AD (2006) Shrinking ponds in subarctic Alaska based on 1950–2002 remotely sensed images. *J Geophys Res* 111:G04002
- Ross HB (1985) An atmospheric selenium budget for the region 30°N to 90°N. *Tellus* 37B:78–90
- Rossi PG, Laurion I, Lovejoy C (2013) Distribution and identity of Bacteria in subarctic permafrost thaw ponds. *Aquat Microb Ecol* 69:231–245
- Saulnier-Talbot E, Pienitz R (2001) Postglacial isolation of a coastal basin near Kuujuaapik-Whapmagostui, Hudsonie: a diatom biostratigraphical investigation. *Geogr Phys Quatern* 55:63–74
- Séby F, Potin-Gautier M, Lespés G, Astruc M (1997) Selenium speciation in soils after alkaline extraction. *Sci Total Environ* 207:81–90
- Sharmasarkar S, Vance GF (1997) Extraction and distribution of soil organic and inorganic selenium in coal mine environments of Wyoming, USA. *Environ Geol* 29:17–22
- Stolz JE, Basu P, Santini JM, Oremland RS (2006) Arsenic and selenium in microbial metabolism. *Annu Rev Microbiol* 60:107–130
- Telmer K, Bonham-Carter GF, Kliza DA, Hall GEM (2004) The atmospheric transport and deposition of smelter emissions: evidence from the multi-element geochemistry of snow, Quebec, Canada. *Geochim Cosmochim Acta* 68:2961–2980
- Tessier E, Amouroux D, Abril G, Lemaire E, Donard OFX (2002) Formation and volatilisation of alkyl-iodides and -selenides in macrotidal estuaries. *Biogeochemistry* 59:183–206
- Tietjen T, Vähätalo AV, Wetzel RG (2005) Effects of clay mineral turbidity on dissolved organic carbon and bacterial production. *Aquat Sci* 67:51–60
- Tolu J, Le Hécho I, Bueno M, Thiry Y, Potin-Gautier M (2011) Selenium speciation analysis at trace level in soils. *Anal Chim Acta* 684:126–133
- Tolu J, Di Tullo P, Le Hecho I, Thiry Y, Pannier F, Potin-Gautier M, Bueno M (2014) A new methodology involving stable isotope tracer to compare simultaneously short- and long-term selenium mobility in soils. *Anal Bioanal Chem* 406:1221–1231
- Turner A, Turner D, Braungardt C (2013) Biomonitoring of thallium availability in two estuaries of southwest England. *Mar Pollut Bull* 69:172–177
- USEPA (2002) National recommended water quality criteria: 2002. EPA-822 R-02-047. Office of Water, Washington, DC
- Vallee S, Payette S (2007) Collapse of permafrost mounds along a subarctic river over the last 100 years (northern Quebec). *Geomorphology* 90:162–170
- Van Dael P, Lewis J, Barclay D (2004) Stable isotope-enriched selenite and selenate tracers for human metabolic studies: a fast and accurate method for their preparation from elemental selenium and their identification and quantification using hydride generation atomic absorption spectrometry. *J Trace Elem Med Biol* 18:75–80

- Velinsky J, Cutter GA (1991) Geochemistry of selenium in a coastal salt marsh. *Geochim Cosmochim Acta* 55:179–191
- Vriens B, Ammann AA, Hagendorfer H, Lenz M, Berg M, Winkel LHE (2014) Quantification of methylated selenium, sulfur, and arsenic in the environment. *PLoS ONE* 9:e102906. <https://doi.org/10.1371/journal.pone.0102906>
- Vriens B, Behra R, Voegelin A, Zupanic A, Winkel LHE (2016) Selenium Uptake and Methylation by the Microalga *Chlamydomonas reinhardtii*. *Environ Sci Technol* 50:711–720
- Watanabe S, Laurion I, Chokmani K, Pienitz R, Vincent WF (2011) Optical diversity of thaw ponds in discontinuous permafrost: a model system for water color analysis. *J Geophys Res* 116:G02003
- Wen H, Carignan J (2007) Reviews on atmospheric selenium: emissions, speciation and fate. *Atmos Environ* 41:7151–7165
- Wen H, Carignan J (2009) Ocean to continent transfer of atmospheric Se as revealed by epiphytic lichens. *Environ Pollut* 157:2790–2797
- Winkel LHE, Johnson CA, Lenz M, Grundl T, Leupin OX, Amini M, Charlet L (2012) Environmental selenium research: from microscopic processes to global understanding. *Environ Sci Technol* 46:571–579
- Yamada H, Hattori T (1990) Determination of soluble selenium in soils. *Soil Sci Plant Nutr* 36:163–166
- Zhang Y, Moore JN (1997) Environmental conditions controlling selenium volatilization from a wetland system. *Environ Sci Technol* 31:511–517
- Zhang T, Barry RG, Knowles K, Heginbottom JA, Brown J (2008) Statistics and characteristics of permafrost and ground-ice distribution in the Northern Hemisphere. *Polar Geogr* 31:47–68

**Publisher's Note** Springer Nature remains neutral with regard to jurisdictional claims in published maps and institutional affiliations.